JOURNAL OF VIROLOGY, Oct. 2009, p. 10480–10493 Vol. 83, No. 20
0022-538X/09/$08.00+0 doi:10.1128/JVI.01195-09

Probing the Spatial Organization of Measles Virus Fusion Complexes▽

Tanja Paal,[1]# Melinda A. Brindley,[1]# Courtney St. Clair,[1]# Andrew Prussia,[2]# Dominika Gaus,[1] Stefanie A. Krumm,[1] James P. Snyder,[2] and Richard K. Plemper[1,3,4]*

Department of Pediatrics, Emory University School of Medicine and Children's Healthcare of Atlanta, Atlanta, Georgia 30322[1]; Department of Chemistry, Emory University, Atlanta, Georgia 30322[2]; and Department of Microbiology & Immunology, Emory University School of Medicine,[3] and Children's Healthcare of Atlanta,[4] Atlanta, Georgia 30322

Received 10 June 2009/Accepted 24 July 2009

The spatial organization of metastable paramyxovirus fusion (F) and attachment glycoprotein hetero-oligomers is largely unknown. To further elucidate the organization of functional fusion complexes of measles virus (MeV), an archetype of the paramyxovirus family, we subjected central predictions of alternative docking models to experimental testing using three distinct approaches. Carbohydrate shielding through engineered N-glycans indicates close proximity of a membrane-distal, but not membrane-proximal, section of the MeV attachment (H) protein stalk domain to F. Directed mutagenesis of this section identified residues 111, 114, and 118 as modulators of avidity of glycoprotein interactions and determinants of F triggering. Stalk-length variation through deletion or insertion of HR elements at positions flanking this section demonstrates that the location of the stalk segment containing these residues cannot be altered in functional fusion complexes. In contrast, increasing the distance between the H head domains harboring the receptor binding sites and this section through insertion of structurally rigid α-helical domains with a pitch of up to approximately 75 Å downstream of stalk position 118 partially maintains functionality in transient expression assays and supports efficient growth of recombinant virions. In aggregate, these findings argue against specific protein-protein contacts between the H head and F head domains but instead support a docking model that is characterized by short-range contacts between the prefusion F head and the attachment protein stalk, possibly involving H residues 111, 114, and 118, and extension of the head domain of the attachment protein above prefusion F.

Paramyxoviruses infect cells through fusion of the viral envelope with target cell membranes. For all members of the *Paramyxovirinae* subfamily, this involves the concerted action of two envelope glycoproteins, the fusion (F) and attachment (H, HN, or G, depending on the *Paramyxovirinae* genus) proteins. Both proteins feature short lumenal tails, a single transmembrane domain, and large ectodomains. The F protein, in type I orientation, forms homotrimers, while homodimers or homotetramers have been suggested as functional units for attachment proteins of different *Paramyxovirinae* subfamily members (7, 14, 28, 41, 49, 50, 66). For entry, upon receptor binding, the attachment protein is considered to initiate a series of conformational rearrangements in the metastable prefusion F protein (15, 77), which ultimately brings together transmembrane domains and fusion peptides and, thus, donor and target membranes (3, 32, 45, 53, 80).

Multiple studies have demonstrated that specific interactions between compatible F and attachment proteins of paramyxovirinae are imperative for the formation of functional fusion complexes (6, 29, 36, 42, 43, 56, 75). However, the molecular nature of these interactions and the spatial organization of functional glycoprotein hetero-oligomers remain largely unknown. Individual ectodomain and partial ectodomain crystal structures have been obtained for different paramyxovirus F (13, 76, 77) and attachment (8, 14, 17, 28, 35, 79) proteins, respectively. For F, a stabilized human parainfluenza virus type 5 (HPIV5) ectodomain that is believed to represent a prefusion conformation folds into a globular head structure that is attached to the transmembrane domains through a helical stalk consisting of the membrane-proximal heptad repeat B (HR-B) domains (77). For the attachment protein, a globular head that harbors the receptor binding sites is considered to be connected to the transmembrane region through extended stalk domains (34, 78). Crystal structures of isolated head domains have been solved for several paramyxovirus attachment proteins, including measles virus (MeV) H, and reveal the six-blade propeller fold typical of sialidase structures (8, 14, 17, 28, 79). However, morbilliviruses recognize proteinaceous receptors (for MeV, the regulator of complement activation [CD46] and/or signaling lymphocytic activation molecule [SLAM], depending on the virus strain) (21, 40, 46, 51, 64, 65). X-ray data do not extend to the stalk domains, but circular dichroism analysis (78) and structure predictions (36, 78) support an α-helical coiled-coil configuration of the stalk.

The nature of individual residues that engage in specific intermolecular interactions between glycoproteins of paramyxovirinae prior to refolding has been studied most extensively for the attachment protein. The stalk domains of several paramyxovirus HN proteins have been implicated in mediating specificity for their homotypic F proteins (18, 20, 43, 63, 70, 72). We have found that this extends to MeV and canine distemper virus H and, thus, to paramyxovirinae recognizing proteinaceous receptors (36), supporting the general hypothesis that F-interacting residues may reside in the stalk region of the attachment protein (30, 78).

* Corresponding author. Mailing address: Division of Infectious Diseases, Department of Pediatrics, 520 Children's Center, 2015 Uppergate Drive, Emory University School of Medicine, Atlanta, GA 30322. Phone: (404) 727-1605. Fax: (404) 727-9223. E-mail: rplempe@emory.edu.

# These authors contributed equally to the study.

▽ Published ahead of print on 5 August 2009.

Considerably less information concerning the nature of F microdomains that mediate attachment protein specificity is available. Among the few exceptions are peptides derived from Newcastle disease virus (NDV) and Sendai virus F HR-B domains, which interact with soluble variants of the respective HN proteins in vitro (25, 67). Multiple domains have been suggested to mediate specificity of HPIV2 F for its HN (69). However, a conclusive N-glycan shielding study (43) and structural information (77, 78) argue against direct contacts between NDV F HR-B domains and HN in native glycoprotein complexes. Thus, the role of individual HPIV2 F residues in HN binding is unclear (25, 43).

Building on the observation that MeV H is able to engage in productive heterotypic interactions with F proteins derived from some but not all isolates of closely related canine distemper virus, we have recently identified residues in morbillivirus F (MeV F residue 121) and H (H stalk residues 110 to 114) that interdependently contribute to physical MeV glycoprotein interaction and F triggering for fusion (36). While these residues could mediate reciprocal glycoprotein specificity through long-range effects, molecular modeling of the MeV H stalk in an α-helical conformation has posited F residue 121 at the same level above the viral envelope as H residues 110 to 114, making direct contacts structurally conceivable (36). This spatial organization of functional fusion complexes furthermore provides a comprehensive explanation for previous demonstrations of a specific role for attachment protein stalk domains of paramyxovirinae in functional and physical interactions with F (18, 43, 63, 70, 72). However, this "staggered-head" model mandates positioning the globular head of the attachment protein above the prefusion F trimer (36), as opposed to a suggested "parallel-head" alignment of the glycoproteins (31, 47). The latter is mostly based on transmission electron microscopy micrographs of viral particles apparently showing glycoprotein spikes of equal length (33). Unfortunately, these images lack the resolution for an identification of the molecular nature of the spikes (attachment or F protein) or the distinguishing between densely packaged H and F head domains of different heights and laterally aligned head domains. Indeed, a recent single-particle reconstruction based on cryo-electron microscopy images of HPIV5 particles revealed that defined spikes correspond to F in a postfusion conformation, which was interpreted as a product of possible premature F refolding (38). These two-dimensional images of heavy-metal-stained particles did not reveal F spikes in a prefusion conformation. Rather, a dense surface layer was considered to correspond to prefusion glycoprotein hetero-oligomers (38). In addition to further-advanced image reconstructions, biochemical assessment of alternative docking modes is imperative for the elucidation of the organization of functional fusion complexes of paramyxovirinae.

In this study, we subjected central predictions of the hypothetical alignment models to experimental analysis. By employing carbohydrate shielding, directed mutagenesis, and variation of the length of the H stalk domain, we examined the proximity of different regions of the H stalk to F, probed a role of individual residues around the previously identified H stalk section from positions 110 to 114 in the formation of functional fusion complexes, tested the effect of varying the length of the H stalk membrane proximal and membrane distal to this section, and explored the general possibility of whether specific contacts between the prefusion F and H head domains are required for F triggering. Experimental data were interpreted in the light of a working model of MeV glycoprotein hetero-oligomers prior to receptor binding.

MATERIALS AND METHODS

Cell culture, transfection, and production of virus stocks. All cell lines were maintained at 37°C and 5% CO_2 in Dulbecco's modified Eagle's medium supplemented with 10% fetal bovine serum. Vero (African green monkey kidney epithelial) cells (ATCC CCL-81) stably expressing human SLAM (Vero-SLAM cells) (52), and baby hamster kidney (BHK-21) cells stably expressing T7 polymerase (BSR-T7/5 [BHK-T7] cells) (10) were incubated at every third passage in the presence of G-418 (Geneticin) at a concentration of 100 μg/ml. Lipofectamine 2000 (Invitrogen) was used for all cell transfections. To prepare MeV stocks, Vero-SLAM cells were infected at a multiplicity of infection (MOI) of 0.001 PFU/cell and incubated at 37°C. Cells were scraped in Opti-MEM (Invitrogen), virus was released by two freeze-thaw cycles, and titers were determined by 50% tissue culture infective dose ($TCID_{50}$) titration according to the Spearman-Karber method (59) as described previously (56). To prepare stocks of modified vaccinia virus Ankara expressing T7 polymerase (60), DF-1 (chicken embryo fibroblast) cells (ATCC CRL-12203) were infected at an MOI of 1.0 PFU/cell, and cell-associated viral particles were harvested 40 h postinfection.

Site-directed mutagenesis, random staggered-priming mutagenesis, and generation of recombinant MeV genomes. Base vectors for all transient MeV glycoprotein expression experiments and directed-mutagenesis approaches were plasmids pCG-F and pCG-H, encoding glycoproteins derived from the MeV Edmonston strain under the control of the constitutive cytomegalovirus promoter (12). For point mutations, heptamer insertions, or heptamer deletions, directed mutagenesis following the QuikChange protocol (Stratagene) was employed using appropriate primers (individual sequences are available upon request). All changes were confirmed by DNA sequencing, and expression of mutagenized proteins was verified by immunoblotting. To generate different-length tandem repeats of the H stalk downstream of stalk nucleotide 351, a staggered-priming mutagenesis strategy was developed. Using a pCG-H variant harboring an additional copy of stalk residues 84 to 90 at residue 118 (H-118▽7x) as the template, mutagenesis was carried out with primer 5′-**cactgacctagtgaaattc**ATAGAACACCAAGTGAAAGAT**atcgagcatcaggtcaagg**, which consists of H stalk nucleotides 333 to 351 (boldface), the HR insertion (uppercase letters), and, for the H-118▽7x template, stalk nucleotides 250 to 268 and 352 to 370 (boldface and underlined), corresponding to amino acids 84 to 90 and the additional copy of this HR inserted at residue 118, respectively. This reaction efficiently (approximately 25 to 50% of clones analyzed) yielded H constructs with extended-length tandem stalk insertions at stalk position 118 (see Fig. 6B for individual sequences). To transfer an H variant harboring a 41-residue stalk elongation (H-118▽41x) into a full-length cDNA copy of the MeV Edmonston genome, a PacI/SpeI fragment containing the H-encoding open reading frame (ORF) was replaced in p(+)MeV-NSe (58) with this variant, resulting in plasmid p(+)MeV-H 118▽41x. An additional stop codon was added to the H-118▽41x ORF to render the resulting genome compatible to the rule-of-six that applies to many members of the paramyxovirus family, including MeV (26). An enhanced green fluorescent protein (eGFP)-encoding ORF was furthermore inserted as an additional transcription unit upstream of the nucleocapsid-encoding ORF through replacement of a PacI/NotI fragment with that derived from p(+)MeV-eGFP (22), resulting in plasmid p(+)MeV-eGFP-H 118▽41x.

Quantification of envelope glycoprotein surface expression. Vero cells were transfected with 2 μg of plasmid DNA encoding MeV H constructs as indicated. After being washed in cold phosphate-buffered saline (PBS), cells were incubated in PBS with 0.5 mg/ml sulfosuccinimidyl-2-(biotinamido)ethyl-1,3-dithiopropionate (Pierce) for 20 min at 4°C, followed by washing and quenching for 10 min at 4°C in Dulbecco's modified Eagle's medium. Samples were lysed in immunoprecipitation buffer, and lysates were cleared by centrifugation for 45 min at 20,000 × *g* and 4°C. Biotinylated proteins were adsorbed to immobilized streptavidin for 120 min at 4°C, washed two times in buffer A (100 mM Tris, pH 7.6, 500 mM lithium chloride, 0.1% Triton X-100) and then buffer B (20 mM HEPES, pH 7.2, 2 mM EGTA, 10 mM magnesium chloride, 0.1% Triton X-100), and incubated in urea buffer (200 mM Tris, pH 6.8, 8 M urea, 5% sodium dodecyl sulfate [SDS], 0.1 mM EDTA, 0.03% bromphenol blue, 1.5% dithiothreitol) for 30 min at 50°C. Samples were then subjected to SDS-polyacrylamide gel electrophoresis (PAGE) and immunoblotting using a polyclonal antiserum directed against the H cytosolic tail (54). For densitometric quantification, immunoblots

were decorated with anti-rabbit IRDye 800CW conjugate (LI-COR) and analyzed using an Odyssey infrared imager and Odyssey software (LI-COR). Amounts of surface steady-state levels of cellular transferrin receptor that were analyzed in parallel using a monoclonal anti-human transferrin antiserum (Zymed) served as an internal standard.

Enzymatic deglycosylation. For PNGase F-catalyzed deglycosylation, H variants were expressed and subjected to surface biotinylation as described above. Following streptavidin pull-down, samples were split into two equal aliquots, proteins were denatured (0.5% SDS, 400 mM dithiothreitol; 95°C for 10 min), and aliquots were subjected to PNGase F deglycosylation (50 mM sodium phosphate, pH 7.5, 1% NP-40; 1 h at 37°C) or mock treatment. All samples were then analyzed by SDS-PAGE and immunoblotting using antiserum directed against the cytosolic H tail.

Expression and purification of soluble SLAM molecules. For expression of a soluble SLAM-murine immunoglobulin G (sSLAM-mIgG) fusion protein, a cDNA sequence encoding the first 233 amino acids of the SLAM ectodomain was isolated through reverse transcription-PCR from Vero-SLAM cells, and the sequence was confirmed. This fragment was subcloned in frame to the 5′ end of an ORF encoding murine IgG heavy chains that is present in the RCASBP(A) vector, a replication-competent retrovirus vector derived from avian leukosis virus (23). After transfection of the RCASBP(A) construct into permissive DF-1 cells, sSLAM-mIgG was purified from culture supernatants (2.5 liters, total volume) through affinity chromatography using immobilized protein G, ultrafiltration, and dialysis against PBS. The final purity of sSLAM-mIgG determined by SDS-PAGE and Coomassie blue staining was ≥90%, and concentrations of purified material were adjusted to 1 mg/ml.

Flow cytometry for analysis of receptor binding capacity. To determine the ability of MeV H variants to bind the SLAM receptor, SLAM- and CD46-negative CHO cells were transfected in a six-well plate format with MeV H constructs (5 μg) and an eGFP expression plasmid (1 μg) as a marker for transfection. Thirty-six hours posttransfection, cells were lifted off and washed twice in PBS supplemented with 3% fetal calf serum. Cell populations were split into two equal aliquots and incubated with either sSLAM-mIgG or a monoclonal antibody mix directed against epitopes in the MeV H ectodomain (Millipore) for 1 h on ice. Following decoration of cells with anti-mouse Fc-specific allophycocyanin conjugate (Jackson Immunoresearch) for 30 min on ice, samples were analyzed using a FACSCanto II cytometer and FlowJo software. Fluorescence intensity was determined for the GFP-positive cell population.

Quantitative cell-to-cell fusion assays. To quantify fusion activity, an effector Vero-SLAM cell population (3×10^5 cells/well) was cotransfected with 2 μg each of H and F expression plasmids, and target Vero-SLAM cells (2×10^5 cells/well) were transfected with 2 μg of the reporter plasmid encoding firefly luciferase under the control of the T7 promoter. Single transfections of plasmids encoding MeV F served as controls. Two hours posttransfection, the effector cells were infected with modified vaccinia virus Ankara expressing T7 polymerase at an MOI of 1.0 PFU/cell. Following incubation for 16 h at 37°C, in the case of effector cells in the presence of 100 μM fusion inhibitory peptide (Bachem), target cells were detached and overlaid on washed effector cells at a 1:1 ratio and incubated at 37°C. Five hours postoverlay, cells were lysed using Bright Glo lysis buffer (Promega), and the luciferase activity was determined using a luminescence counter (PerkinElmer) and the Britelite reporter gene assay system (PerkinElmer). The instrument's arbitrary values were analyzed by subtracting the relative background provided by values of the controls, and these values were normalized against the reference constructs indicated in the figure legends. On average, background values were <1.5% of the values obtained for reference constructs.

Envelope glycoprotein cross-linking and immunoprecipitation. Vero-SLAM cells were transfected with 4 μg each of plasmid DNA encoding MeV F and H variants as specified for the individual experiments and incubated in the presence of 100 μM fusion inhibitory peptide. At 36 h posttransfection, cells were washed three times with cold PBS and treated with DTSSP (1 mM final concentration in PBS) for two hours at 4°C, followed by the addition of Tris, pH 7.5, to a final concentration of 20 mM for quenching (15 min, 4°C). Cells were then lysed in radioimmunoprecipitation assay buffer (1% sodium deoxycholate, 1% NP-40, 150 mM NaCl, 50 mM Tris-Cl, pH 7.2, 10 mM EDTA, 50 mM NaF, 0.05% SDS, protease inhibitors [Roche], 1 mM phenylmethylsulfonyl fluoride), and cleared lysates (20,000 × *g*; 30 min at 4°C) were incubated with specific antibodies directed against epitopes in the MeV H ectodomain (Millipore) at 4°C. After precipitation with immobilized protein G at 4°C, samples were washed two times each in buffers A and B as described above, eluted in urea buffer, and subjected to SDS-PAGE and immunoblotting. Coprecipitated F was visualized in a Chemi-Doc XRS digital imaging system (Bio-Rad) using a polyclonal antiserum against the F cytosolic tail (37) and rabbit IgG light chain-specific horseradish peroxidase conjugate. For densitometry, signals were quantified using the QuantityOne software package (Bio-Rad).

Recovery of recombinant MeV. Recombinant MeV was generated as described previously (58) with the following modifications: BHK-T7 cells were cotransfected by calcium phosphate precipitation with a plasmid carrying a cDNA copy of the recombinant MeV genome and plasmids encoding the MeV L, N, or P protein. All constructs were under the control of the T7 promoter. Helper cells were overlaid on Vero-SLAM cells 76 h posttransfection, and emerging virus particles were transferred to fresh Vero-SLAM cells. The integrity of recombinant MeV particles was then confirmed by reverse transcription-PCR and DNA sequencing of the modified area using Superscript II reverse transcriptase and random hexamer primers for first-strand synthesis.

Virus growth curves. For multistep growth curves, cells were infected in a six-well-plate format with recombinant MeV Edmonston (recMeV-Edm) variants as specified at an MOI of 0.001 PFU/cell. To ensure equal MOIs for each variant analyzed, all input stocks were prediluted to approximately 10^4 $TCID_{50}$/ml in Opti-MEM (Invitrogen) prior to infection, and titers were reconfirmed by $TCID_{50}$ titration. Sixty minutes postinfection, inocula were replaced with fresh growth medium. Cell-associated viral particles were harvested every 12 h as described above and subjected to $TCID_{50}$ titration. For documentation of the viral cytopathic effect (CPE), plates were photographed at a magnification of ×200.

Molecular modeling. Previously described structural models of MeV F and H proteins were used in this analysis (36, 57). Briefly, a homology model of the MeV F protein was built on the basis of the coordinates reported for the prefusion HPIV5 F X-ray crystal structure (77). The MeV H structural model was built by connecting the X-ray coordinates available for residues 154 to 607 forming the head domain (14, 28) to a coiled-coil model of the MeV H stalk (residues 58 to 153), which was generated by mapping these residues on the α-helical scaffold of cortexillin I (11) as described previously (36). In the present study, a slightly different mapping of the stalk residues was used to better accommodate the stutter in the HR sequence at residues I99 and L105. A single-residue gap was introduced in the alignment after P108, placing this residue in "a" position of the helical wheel. Proline residues 94 and 127 are also expected to introduce kinks in the helix structure in agreement with electron microphotographs of the related HPIV5 HN (78). Due to the lack of native X-ray information, however, these are not represented in the schematic models. For the modeling of N-glycan additions, a sugar with the following structure was prepared in three dimensions by using Maestro software (Schrodinger, LLC, New York, NY): asparagine-GlcNAc-β(1,4)-GlcNAc-β(1,4)-Man[-α(1,3)-Man-β(1,2)-GlcNAc-β(1,4)-Gal-α(2,6)-NeuNAc] [-α(1,6)-Man-β(1,2)-GlcNAc-β(1,4)-Gal-α(2,6)-NeuNAc]. For a reasonable low-energy conformation of the carbohydrate, a Monte Carlo conformational search of 1,000 steps was performed with MacroModel 9.5 software (Schrodinger, LLC, New York, NY) using the OPLS2005 force field with generalized Born/surface area water solvation. The low-energy conformation was attached to the proteins by superimposing the backbone atoms of asparagine to the target glycosylation position on the MeV H stalk. Structural models of MeV H stalk deletion mutants were generated by removing HR regions from the stalk model, save for one flanking residue on either side of the deletion (residues 85 to 89 for HR 84 to 90 and residues 119 to 123 for HR 118 to 124). The flanking residues were then used to superimpose the backbone atoms of the downstream structure to the upstream structure, generating one construct (H-Δ84-90) with residues 58 to 83 attached to residues 91 to 607 and another construct (H-Δ118-124) with residues 58 to 117 attached to residues 125 to 607. MeV H stalk insertions were generated by duplicating the desired section of the stalk plus one flanking residue on either side for superimposing (residues 83 to 91, 117 to 125, and 83 to 118). These duplicate sections were inserted into the downstream structure and aligned by superimposing the backbone atoms of the overlapping residues. The upstream structure was then superimposed in the same manner to the C-terminal end of the newly extended stalk, generating the constructs H-84▽7x, H-118▽7x, and H-118▽41x.

RESULTS

With the overarching goal of further elucidating the spatial organization of paramyxovirus envelope glycoproteins in a prefusion state, we subjected key predictions of hypothetical docking models to experimental testing.

Engineering of N glycosylation sites into the H stalk. Independently of the lateral arrangement of the head domains, schematic juxtapositions of F and H structures predict that

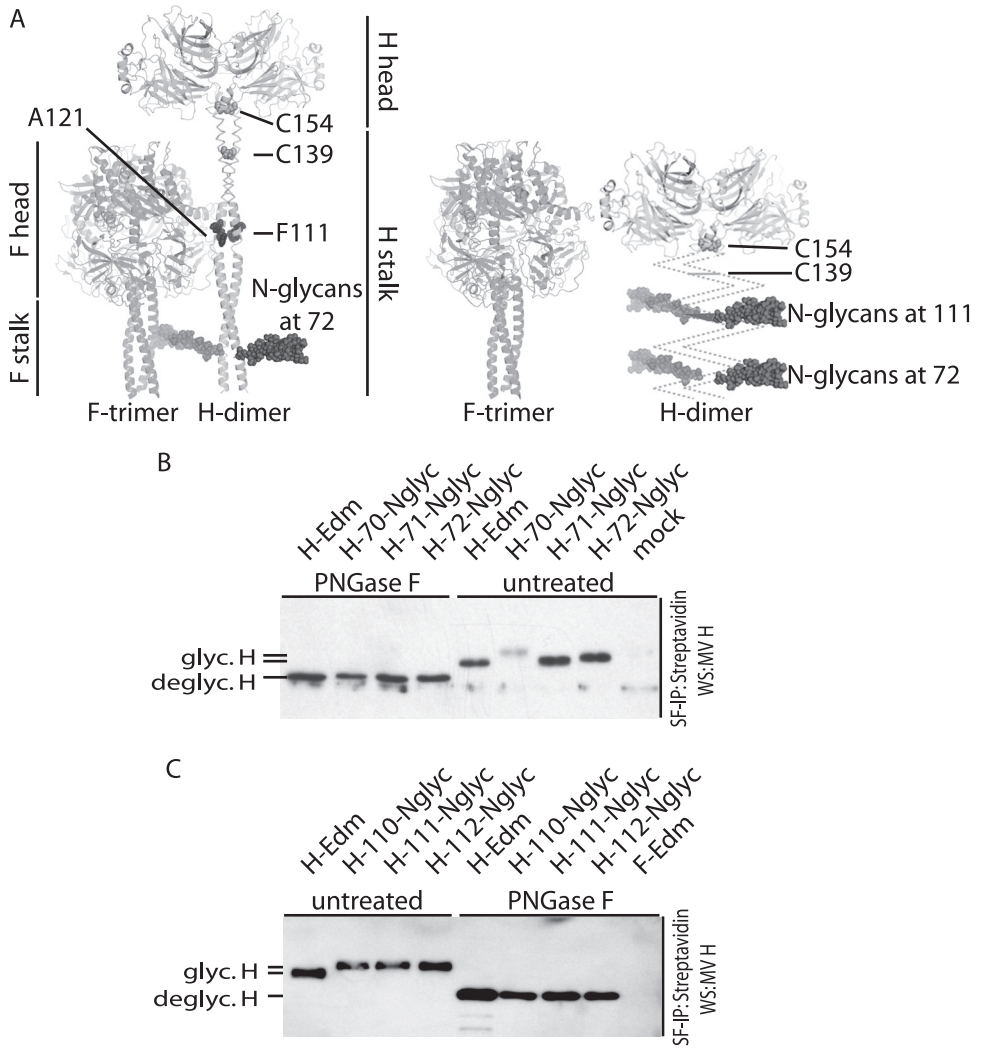

FIG. 1. Insertion of additional N-glycans into the MeV H stalk domain at membrane-proximal and membrane-distal positions. glyc., glycosylated; deglyc., deglycosylated. (A) Ribbon representation of hypothetical envelope glycoprotein interaction modes and the positions of additional N-glycans engineered to probe the proximity of the F trimer to H. Staggered alignment (left panel) predicts that only N-glycans added at a membrane-proximal position (shown as dark spheres for H residue 72) but not a membrane-distal position (highlighted residue 111; engineered N-glycan not shown for spatial constraints) are compatible with the formation of functional fusion complexes. Parallel alignment of the head domains (right panel) permits H and F hetero-oligomerization with added N-glycans at either position in the H stalk (shown for residues 72 and 111 as dark spheres). Prefusion F and H head and stalk domains, F residue A121 (previously identified to contribute to MeV H and F interaction) (36), and cysteine residues in the H stalk (C139 and C154) engaged in disulfide bonds for covalent H dimerization are shown. H is represented as a dimer in accordance with available X-ray information, although a tetramer (dimer-of-dimers) may in fact be the physiological oligomer. Either order is predicted to tolerate additional N-glycans at position 72. (B) Of three N-glycosylation sites engineered at positions 70, 71, and 72, only that at position 72 is efficiently glycosylated and surface expressed. Surface-exposed proteins were biotinylated, precipitated with immobilized streptavidin, and subjected to PNGase F treatment for deglycosylation or mock treated in equal aliquots. Electrophoretic mobility of MeV H species was determined by SDS-PAGE and decoration of immunoblots with a specific antiserum directed against the cytosolic tail of MeV H. (C) Engineered N-glycans at positions 110, 111, and 112 are efficiently recognized. Treatment of samples was as described for panel B.

membrane-proximal regions of the H stalk are not in direct contact with the F trimer. For membrane-distal stalk sections, however, the staggered-head (Fig. 1A, left panel), but not the parallel-head model (Fig. 1A, right panel), implies close proximity of the prefusion F head domain. Carbohydrate shielding through insertion of additional N-glycosylation sites is reportedly capable of examining the contribution of protein domains to activity (24, 68) and has been used in a conclusive study to test candidate contact zones between NDV HN and F (43). We employed this strategy to probe the proximity of F from the H stalk domain at a membrane-proximal and membrane-distal position. Since the exact rotational orientation of the H stalk is unknown, N-glycosylation sites were introduced separately for each position at three consecutive residues: residues 70 to 72 were chosen as targets for membrane-proximal N-glycans guided by the prediction of the staggered-head model that carbohydrates at these positions will not impair the interaction of H with F, and residues 110 to 112 were chosen for mem-

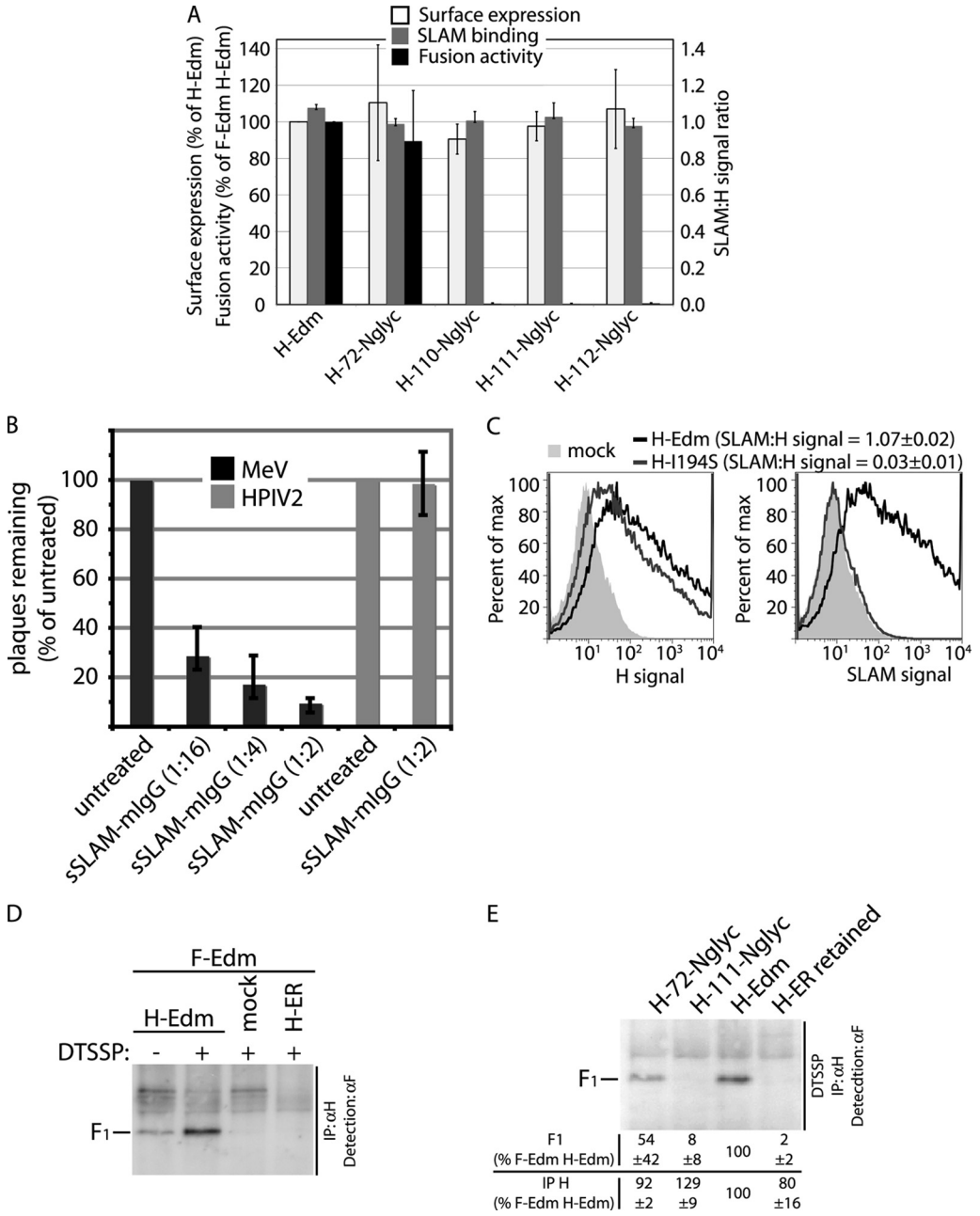

FIG. 2. Additional N-glycans at H stalk position 72, but not 110, 111, or 112, allow the formation of functional H-F fusion complexes. (A) Assessment of surface expression, SLAM binding capacity, and cell-to-cell fusion activity of H variants. Surface expression was determined through surface biotinylation using transferrin receptor as an internal standard. SLAM binding was monitored as detailed for panel B. Flow cytometry values are expressed as ratios of SLAM signal to H signal. Fusion activity was determined in a firefly luciferase-based quantitative fusion assay upon coexpression of H variants with Edmonston F (F-Edm). In all cases, values are expressed relative to unmodified H-Edm and represent the averages from at least three independent experiments ± SEMs. (B) Virus neutralization assay confirming specific interaction of purified, sSLAM, C-terminally fused to mIgG heavy chains (sSLAM-mIgG), with MeV. Virus particles were incubated with dilutions of purified sSLAM-mIgG as specified for 30 min at 25°C, followed by transfer to Vero-SLAM target cells and agar overlay. Plaque counts were determined 72 h postinfection. Counts of equally sSLAM-mIgG-treated HPIV2-induced plaques were not altered by sSLAM-mIgG, confirming specificity of the interaction. Values show plaque counts relative to vehicle (PBS)-treated controls and reflect averages from three independent experiments ± SDs. (C) Assessment of SLAM binding capacity. MeV receptor-negative CHO cells expressing H variants were analyzed by flow cytometry using an sSLAM-mIgG fusion protein or mouse monoclonal antibodies directed against epitopes in the MeV H ectodomain and a mouse-specific allophycocyanin conjugate. Numbers represent the ratios of mean fluorescence intensities obtained after decoration of cells with sSLAM-IgG (SLAM signal) or anti-H antibodies (H signal). Averages from three independent experiments ± SEMs are shown. max, maximum. (D) Chemical cross-linking stabilizes surface-exposed H-Edm/F-Edm hetero-oligomers in situ prior to cell lysis. Cells transfected with equal amounts of H-Edm- and F-Edm-expressing plasmids were treated with the membrane-impermeable, reducible cross-linker DTSSP, followed by quenching and lysis with stringent radioimmunoprecipitation assay buffer. For controls, DTSSP was omitted, cells were transfected with F-Edm-expressing plasmids only or cells were cotransfected with F-Edm and an H-Edm variant harboring a cytosolic endoplasmic reticulum retention motif (H-ER) (55). For immunoprecipitation (IP), a monoclonal antibody cocktail directed against epitopes in the MeV H ectodomain (αH) was used, followed by

brane-distal N-glycans based on our previous identification of the role of MeV H section 110 to 114 in mediating F specificity (36).

Of the membrane-proximal set, only the engineered site at position 72 was recognized efficiently without affecting intracellular transport competence, as demonstrated by comparing the electrophoretic mobilities of these H variants with that of standard H before and after PNGase F deglycosylation of cell surface-exposed material (Fig. 1B). Subsequent full characterization was therefore limited to the corresponding variant, H-72-Nglyc. Equivalent analysis of the electrophoretic mobility of the membrane-distal set confirmed glycosylation at each of the targeted positions, 110, 111, and 112 (Fig. 1C). Recognition of the engineered glycosylation sites was highly efficient for all four constructs, since immunoblotting revealed homotypic mobility patterns that lacked subspecies with Edmonston H (H-Edm)-like mobility prior to PNGase F treatment.

Carbohydrate shielding at a membrane-distal, but not membrane-proximal, position of the H stalk interferes with the formation of functional fusion complexes. Assessments of plasma membrane steady-state levels through surface biotinylation and of SLAM binding through flow cytometry demonstrated essentially unchanged intracellular transport competence and ability to interact with SLAM receptor for all four H variants with engineered N-glycans (Fig. 2A). To establish a receptor binding assay, we generated an sSLAM-mIgG fusion protein that specifically blocks MeV entry, confirming its ability to bind MeV H (Fig. 2B). Figure 2C exemplifies that, following binding of this sSLAM-IgG construct to H-expressing cells by flow cytometry, the ratios of SLAM-specific mean fluorescence intensity to H-specific mean fluorescence intensity provide an assessment of receptor (SLAM) binding competence. For a control, an I194S mutant (H-I194S) that reportedly is unable to bind to SLAM was assessed (48). This construct returned a SLAM-to-H signal ratio of 0.03, compared to 1.07 obtained for standard H (Fig. 2C), confirming specificity of the assay.

Quantification of cell-to-cell fusion using a luciferase reporter-based content mixing assay demonstrated that fusion activity and, thus, F triggering were virtually unaffected by the additional N-glycan at H stalk position 72 (Fig. 2A). In contrast, N-glycans at position 110, 111, or 112 completely blocked F triggering (Fig. 2A), as implied by Fig. 1A.

To assess whether this lack of functionality extends to altered physical interaction of the glycoproteins, we further advanced a coimmunoprecipitation (co-IP) assay that we have previously developed for MeV H and F (36, 55, 56). The general strategy of coprecipitating one envelope glycoprotein with antibodies directed against the other after lysis of the producer cells has been applied to multiple members of the paramyxovirus family (2, 5, 19, 44, 75). However, in this setup, the possibility that removal of the stabilizing lipid bilayer induces conformational changes in the metastable prefusion F trimer (76) prior to co-IP, potentially distorting results, cannot be excluded. To assess envelope glycoprotein hetero-oligomers in situ prior to membrane lysis, we examined membrane-impermeable chemical cross-linkers. Covalently linking surface-expressed MeV glycoprotein hetero-oligomers with membrane-impermeable, reducible DTSSP prior to membrane extraction, immunoprecipitation of H under stringent conditions, and detection of coprecipitated F allowed specific analysis of plasma membrane-embedded envelope glycoprotein complexes (Fig. 2D). Having established this assay, we found that N-glycans at stalk position 111 (representative of N-glycan-mediated shielding of membrane-distal stalk positions) essentially block the formation of functional fusion complexes ($<10\%$ of those observed for unchanged H and F). This observation underscores the concept that DTSSP-mediated MeV glycoprotein cross-linking does not generate artificial H and F complexes. In contrast, N-glycans at position 72 still allow glycoprotein interaction, although at a reduced level compared to standard complexes (Fig. 2E).

These data demonstrate that insertion of additional N-glycans at a membrane-proximal or -distal position of the H stalk does not result in a loss of receptor binding capacity or intracellular protein retention through gross H misfolding. The block of F triggering and glycoprotein hetero-oligomerization by membrane-distal, but not membrane-proximal, N-glycans indicates close proximity of this H stalk section to F.

H residues 111, 114, and 118 are determinants for F triggering. To assess whether a specific subset of residues in the previously identified linear H stalk segment from positions 110 to 114 determines effective F triggering, we next subjected this domain to alanine-scanning mutagenesis. In a first round, all five residues or only the first three or last two residues were mutagenized. The surface expression and SLAM binding ability of these H variants were unchanged, but none was capable of triggering F in cell-to-cell fusion assays (Fig. 3). This extends the essential role of the segment in F triggering to homotypic MeV glycoprotein pairs and indicates that residues in both subsections examined individually (positions 110 to 112 and positions 113 and 114) are required for the formation of functional fusion complexes.

Subsequent single-residue mutagenesis revealed a complete loss of F triggering by H-F111A and a significant reduction by H-L114A, while changes at each of the other three positions (110, 112, and 113) did not affect fusion activity ($\geq 85\%$ of F triggering by standard H; Fig. 4A). We note that H-F111A and H-L114A showed essentially unaltered surface expression, while approximately 20% (H-T112A and H-D113A) to 30%

cleavage of the linker through reducing denaturation buffer, SDS-PAGE, and detection of coprecipitated F protein on immunoblots with a specific antiserum directed against the F protein cytosolic tail. In the absence of DTSSP, the majority of hetero-oligomers dissociates during cell lysis and immunoprecipitation. Cross-linking of proteolytically matured F material and lack of F cross-linking with the ER-retained H variants confirm membrane impermeability of the linker and analysis of surface-exposed complexes. (E) Co-IP of surface-exposed, proteolytically matured MeV F with MeV H with a monoclonal antibody cocktail directed against the MeV H ectodomain after treatment of cotransfected cells with the membrane-impermeable cross-linker DTSSP. For a control, an H variant carrying a cytosolic ER retention motif (H-ER retained) (55) was included. Values show efficiencies of F co-IP (top row) and, for a control, direct H immunoprecipitation (IP; bottom row). They are expressed relative to H-Edm and represent averages from four (co-IP) or at least three (direct immunoprecipitation) independent experiments ± SEMs.

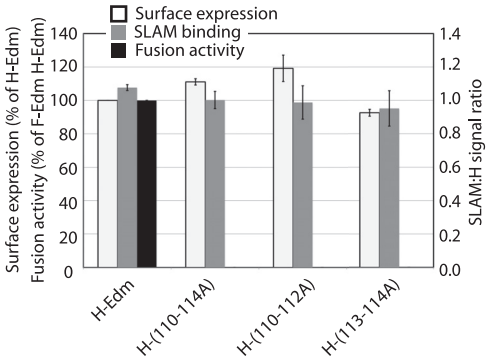

FIG. 3. Integrity of the MeV H stalk microdomain from positions 110 to 114 is required for the formation of functional fusion complexes but not H surface expression or SLAM binding. Alanine-scanning mutagenesis was followed by sample analysis as described in the legend to Fig. 2A. Values represent the averages from at least three independent experiments ± SEMs.

(H-R110A) reductions were observed for the F triggering-competent mutants (Fig. 4A). SLAM binding levels of all variants were equivalent to that of standard H (Fig. 4A).

A three-residue distance between individual positions determining F triggering supports the predicted helical character of the attachment protein stalk domains of paramyxovirinae (36, 43, 78), since an α-helical configuration positions residues 111 and 114 in immediate proximity on consecutive turns of the helix (Fig. 4B). To explore whether neighboring residues on preceding or subsequent turns likewise contribute to F triggering, we extended the alanine mutagenesis to stalk positions 108, 117, 118, and 122, which are predicted to be located at the same face of the helix as residues 111 and 114 (Fig. 4B). Of these, an I118A mutation likewise abolished fusion activity but did not reduce surface expression or SLAM binding capacity (Fig. 4A). None of the other changes resulted in major reductions of F triggering or SLAM binding, although the proline-to-alanine change at position 108 caused an approximately 50% reduction in surface expression (Fig. 4A). In addition to affecting F triggering, the individual mutation of residue 114 or, in particular, 111 or 118 to alanine impaired physical glycoprotein interaction at the plasma membrane (Fig. 4C).

Taken together, these data identify H stalk positions 111, 114, and 118, but not intermittent or flanking residues 108, 112, 113, 117, or 122, as determinants for the formation of functional fusion complexes between MeV H and F. This is consistent with an α-helical configuration of the stalk domains in situ, supporting previous results derived from secondary structure predictions and in vitro analysis of soluble attachment protein ectodomain fragments (36, 43, 78).

H variants with a stalk elongation downstream of residue 118 functionally interact with F. The N-glycan shielding and cross-linking results are compatible with close proximity between F and the H stalk section including residues 111, 114, and 118. The corresponding alignment of F and H (staggered-head model) shown in Fig. 5A implies that shortening the stalk domain will likely disturb glycoprotein hetero-oligomerization due to steric interference of a lowered H head with F. In contrast to the parallel-head model, the staggered-head alignment furthermore predicts that stalk elongation distal, but not

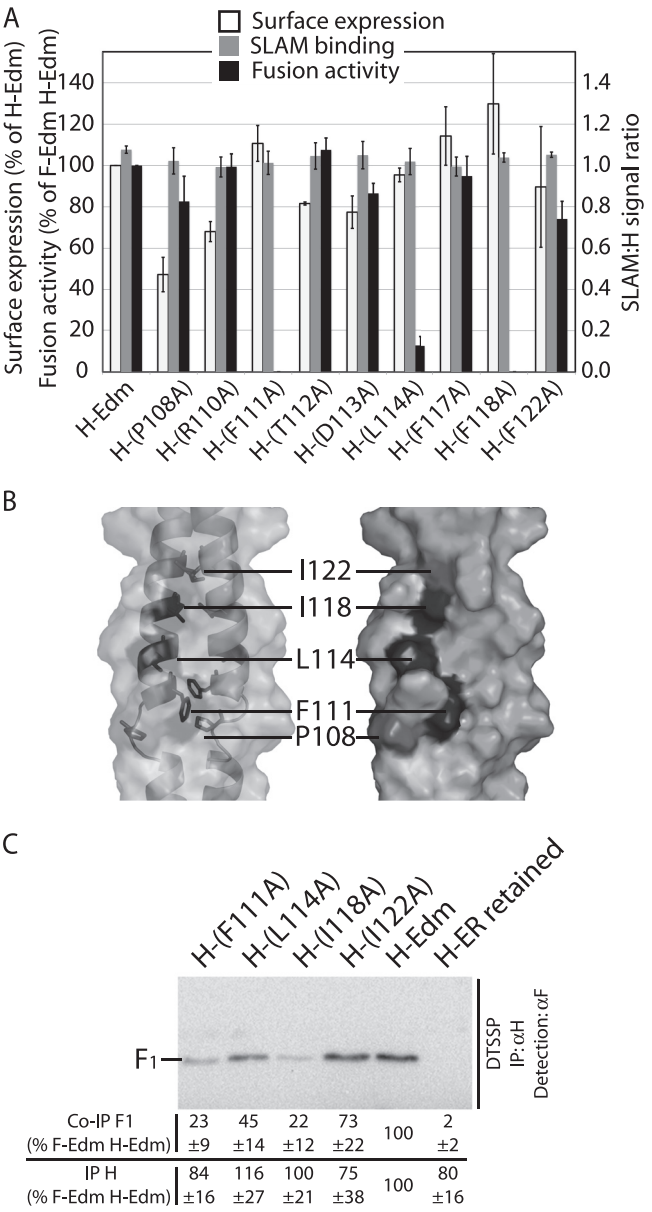

FIG. 4. H stalk residues 111, 114, and 118 are determinants for physical and functional interaction of MeV H and F. F-Edm, MeV Edmonston F. (A) Characterization of H variants harboring individual alanine point mutations as in Fig. 2A. Values represent the averages from at least three independent experiments ± SEMs. Only mutation of residue 111, 114, or 118 substantially reduces F triggering activity. (B) In an α-helical configuration of the H stalk, residues 111, 114, and 118 are predicted to be located adjacent to each other on consecutive turns of the helix. Solvent-accessible surface models of H stalk dimers cover positions 103 to 125. Side chains of residues 111, 114, and 118 are shown in dark gray, and side chains of residues 108 and 122 are shown in light gray. The translucent surface with a ribbon trace (left panel) reveals a possible helix break at P108, making residue 111 accessible (orientation toward the viewer). The opaque surface (right panel) reveals that side chains of residues 111, 114, and 118 form a continuous patch. (C) Co-IP of surface-exposed, matured MeV F with MeV H after DTSSP cross-linking as in Fig. 2E. Values represent averages from four independent experiments ± SEMs. H-ER retained, an H variant carrying a cytosolic endoplasmic reticulum retention motif; IP, immunoprecipitation; αH and αF, antibodies to H and F, respectively.

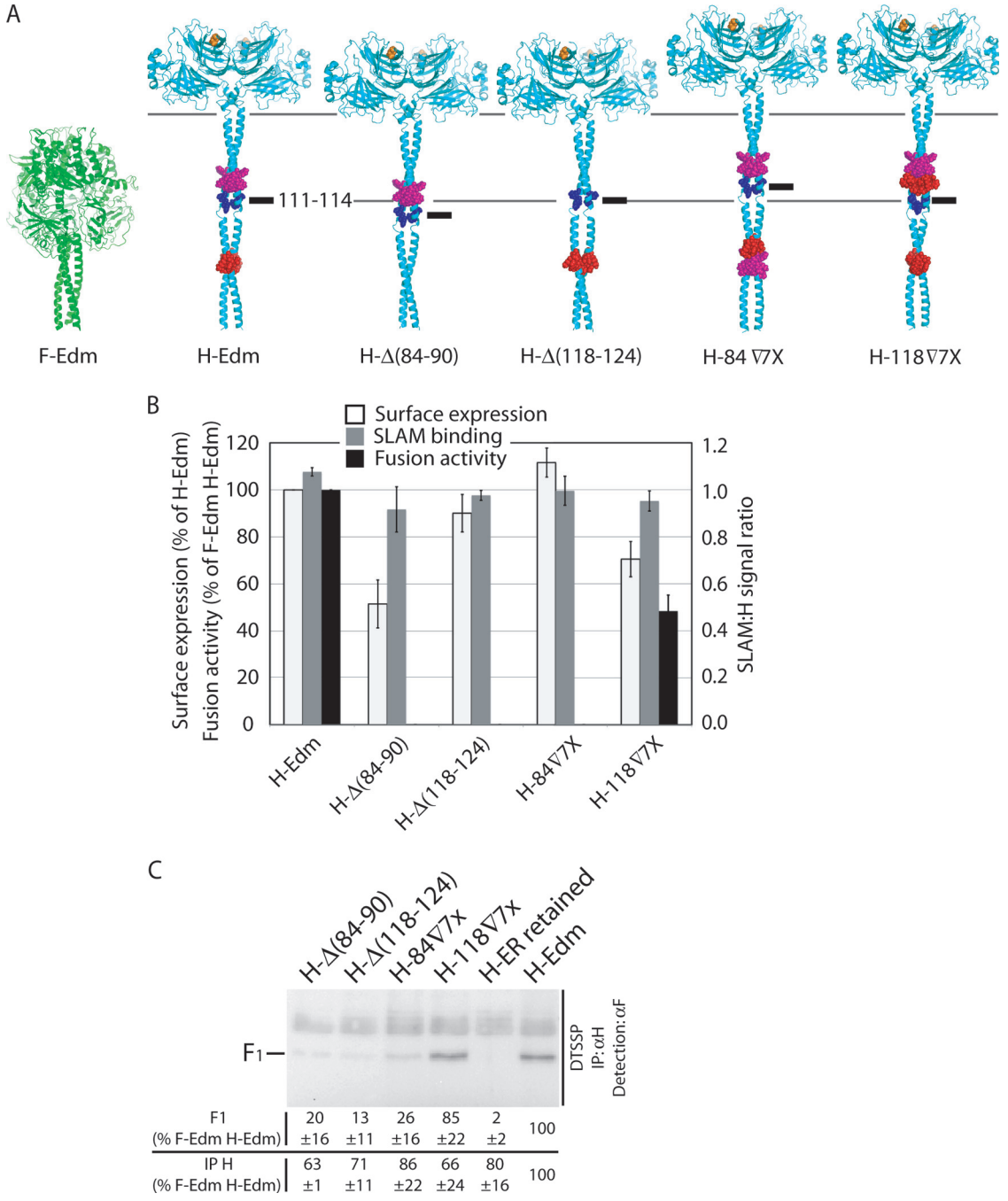

FIG. 5. Insertion of a HR element into the H stalk downstream of position 118 is compatible with functional glycoprotein interaction. F-Edm, MeV Edmonston F. (A) Graphic representation of predicted consequences of H stalk deletions or insertions in a hypothetical hetero-oligomer organization that involves short-range contacts between the prefusion F head and the H stalk. Ribbon models of prefusion MeV F and H (stalk residues 58 to 122 in an α-helical configuration) were aligned at the transmembrane domains as previously described (36). HR elements 118 to 124 (magenta) and 84 to 90 (red) were either individually deleted [H-Δ(118-124) or H-Δ(84-90)] or inserted as an additional copy at residue 84 (H-84∇7x) or 118 (H-118∇7x). The position of residues 111 to 114 (blue; black alignment bars) and alignment guides for this section and the H head domains (horizontal gray lines) are shown. (B) Characterization of the stalk deletion and insertion variants as in Fig. 2A. Values represent the averages from at least three independent experiments ± SEMs. Only the construct with a membrane-distal insertion (H-118∇7x) shows F triggering activity. (C) Co-IP of surface-exposed, matured MeV F with MeV H after DTSSP cross-linking as in Fig. 2E. Values represent averages from four independent experiments ± SEMs. H-ER retained, an H variant carrying a cytosolic endoplasmic reticulum retention motif; IP, immunoprecipitation; αH, antibody to H.

proximal, to residues 111/114/118 should be tolerated, since the relative positions of contacting domains proximal to residue 118 would likely be preserved (Fig. 5A). Deleting or inserting complete HR domains is anticipated to minimally compromise the predicted overall helical conformation of the stalk while altering its length by approximately 11 Å per HR domain.

To test these predictions, we identified two HRs (residues 84

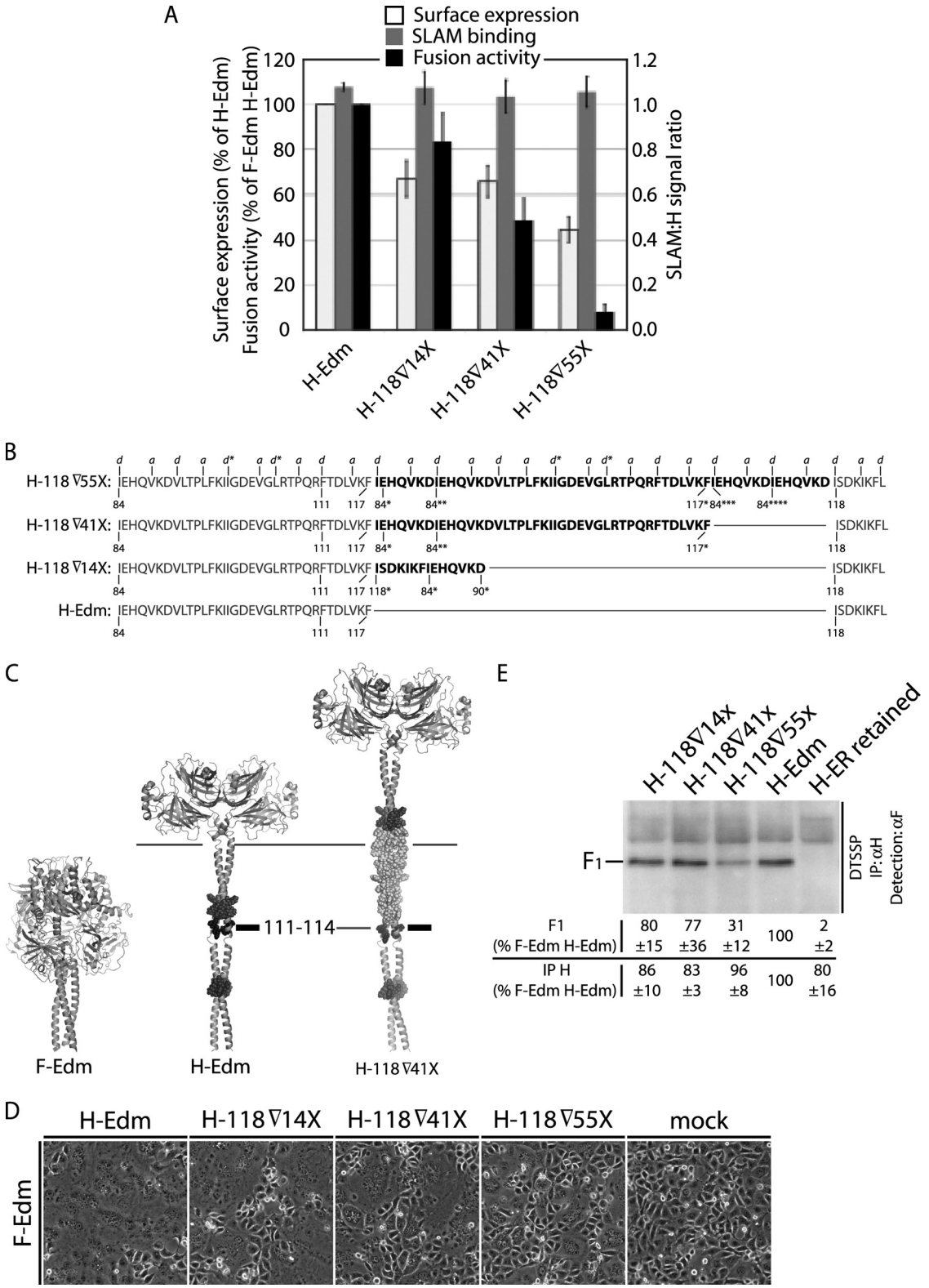

FIG. 6. Membrane-distal insertion of multiple HR elements is compatible with F triggering. F-Edm, MeV Edmonston F. (A) Characterization of H variants harboring stalk insertions at position 118 of 14 (H-84∇14x)-, 41 (H-84∇41x)-, or 55 (H-84∇55x)-residue-insertion variants as in Fig. 2A. Values represent the averages from at least three independent experiments ± SEMs. All constructs show F triggering activity, albeit at a substantially reduced rate in the case of H-84∇55x, harboring the 55-residue insertion. (B) Sequences of H-84∇14x, generated through conventional directed mutagenesis, and H-84∇41x and H-84∇55x, generated through staggered-priming mutagenesis (shown in boldface for each construct). The sequence of unmodified H-Edm is shown in gray, and the positions of residue 84 in additional copies of the HR from positions 84 to 90 (84*, 84**, 84***, and 84****) or residue 118 in additional copies of the HR from positions 118 to 124 (118*), residues 111 and 117, and

to 90 and residues 118 to 124) (Fig. 5A; for amino acid sequences, see Fig. 6B) that flank the 111/114/118 section and are distinct from H residues 91 to 105. Introducing mutations in the latter section was avoided, since this reportedly affects F triggering either through long-range effects or a shared role of this segment and other segments in the formation of functional fusion complexes (16). Our approach furthermore preserved the hydrophobic nature of residue 84, which was likewise identified by Corey and Iorio in the same study to be required for F triggering (16).

Four constructs were generated: constructs with a deletion of the HR from positions 84 to 90 [H-Δ(84-90)] or 118 to 124 [H-Δ(118-124)] or an insertion of an additional copy of the HR from positions 118 to 124 at residue 84 (H-84▽7x) or the HR from positions 84 to 90 at residue 118 (H-118▽7x). The isoleucine residue at position 118 was conserved in all of these, with the exception of H-Δ(118-124), in which, however, an I118L change maintained the hydrophobic nature at position 118. All H variants reached the surface, although plasma membrane steady-state levels of H-118▽7x and H-Δ(84-90) were reduced by approximately 30 and 50%, respectively (Fig. 5B). All four constructs were fully capable of SLAM binding (Fig. 5B). However, microscopic analysis (data not shown) and quantitative fusion assays revealed that both HR deletions and the membrane-proximal HR insertion completely abrogated F triggering. In contrast, stalk elongation membrane-distal of the 111/114/118 section still allowed the formation of functional fusion complexes, since coexpression of H-118▽7x with F resulted in approximately 50% fusion activity of standard H and F (Fig. 5B). Likewise, only stalk elongation downstream of 111/114 (H-118▽7x) was compatible with glycoprotein hetero-oligomerization, whereas membrane-proximal insertion (H-84▽7x) and HR deletions at either position essentially abolished glycoprotein interactions (Fig. 5C).

These results demonstrate that the overall stalk lengths can be increased, but the distance between the transmembrane domain and stalk section from positions 91 to 118 must be preserved for effective hetero-oligomerization and F triggering.

Extensive stalk insertions argue against specific contacts between H and F head domains. F triggering by H-118▽7x suggests that H domains downstream of residue 118 do not engage in functional protein-protein contacts in prefusion hetero-oligomers, thus, further arguing against a parallel-head alignment and indicating a lack of functional contacts between the base of the H and the top of the F head in staggered alignment. Alternatively, structural flexibility of the carboxy-terminal third of the stalk (residues 118 to 154) could compensate for the single HR insertion of the H-118▽7x variant.

To probe these alternatives, we further extended the stalk domain membrane distal to position 118. Insertion of a second additional HR domain generated variant H-118▽14x, with a predicted added stalk length of approximately 22 Å. Compared to H-118▽7x, the second HR domain addition returned very similar surface expression (approximately 70%) of H-Edm, was fully capable of SLAM binding, and improved F triggering to approximately 80% of the standard H value in cell-to-cell fusion assays (Fig. 6A). In parallel to our study of stalk extensions of defined length, we developed a staggered-priming mutagenesis strategy to create different-length tandem repeats of H stalk section 84 to 117, always inserted at position 118. This convenient approach yielded two additional H variants (sequences shown in Fig. 6B) that harbor 41-residue (H-118▽41x) and 55-residue (H-118▽55x) stalk elongations. The two constructs were fully capable of SLAM binding and showed plasma membrane steady-state levels of approximately 65% and 45% of standard H, respectively (Fig. 6A). Remarkably, coexpression of F with H-118▽41x, featuring stalk extensions of nearly 50% of the original lengths (depicted in Fig. 6C), returned approximately 50% fusion activity of standard H. A drastic reduction in F triggering was found for H-118▽55x. However, microphotographs of cells coexpressing this variant and F (Fig. 6D) and cell-to-cell fusion assays confirmed some residual activity, equivalent to approximately 10% of the standard H value (Fig. 6A). As suggested by these findings, all three H variants are capable of physically engaging F. While an approximately 70% reduction of hetero-oligomer formation was observed for H-118▽55x, co-IP efficiencies of H-118▽14x and H-118▽41x with F were similar (nearly 80%) to that observed for H-Edm (Fig. 6E).

In aggregate, these findings demonstrate that membrane-distal insertion into the H stalk of a structurally rigid 41-amino-acid domain composed of consecutive HRs, which is equivalent to a pitch of approximately 75 Å in an α-helical configuration, is largely compatible with the formation of functional fusion complexes.

H variants with a large stalk insertion are functional in the context of virus infection. The remarkable nature of these findings raised the question of whether tolerance of the 41-residue insertion is limited to inducing cell-to-cell fusion in a transient glycoprotein expression setting or extends to sustaining viral entry and efficient production of infectious particles. To test this, we generated a cDNA copy of the MeV Edmonston genome that harbored the H-118▽41x gene in place of the standard H gene and, to facilitate detection of recombinant virions, an eGFP gene as an additional transcription unit.

recMeV-eGFP-(H-118▽41x) virions were recovered successfully and subjected to analysis of CPE in cell monolayers

residues at the termini of the stalk duplications (90* and 117*) are indicated. Markings above the sequences represent the predicted "a" and "d" positions in the stalk helical wheel, and d* indicates HR stutters. (C) Graphic representation of elongated stalk H variant H-84▽41x in comparison with H-Edm. The 41-residue insertion is shown in the predicted helical configuration in light gray. Alignment with F, marking of individual residues and microdomains, and alignment bars are as described in the legend to Fig. 5A. (D) Microphotographs of Vero-SLAM cells cotransfected with 3 μg (each) of expression plasmids encoding F-Edm, H-Edm, or H variant H-84▽14x, H-84▽41x, or H-84▽55x as specified. Mock-transfected cells received F-Edm expression plasmids only. Photographs were taken 15 h posttransfection at a magnification of ×200. Representative fields of view are shown. (E) Co-IP of surface-exposed, matured MeV F with MeV H after DTSSP cross-linking as in Fig. 2E. Values represent averages from four independent experiments ± SEMs. H-ER retained, an H variant carrying a cytosolic endoplasmic reticulum retention motif; IP, immunoprecipitation; αH, antibody to H.

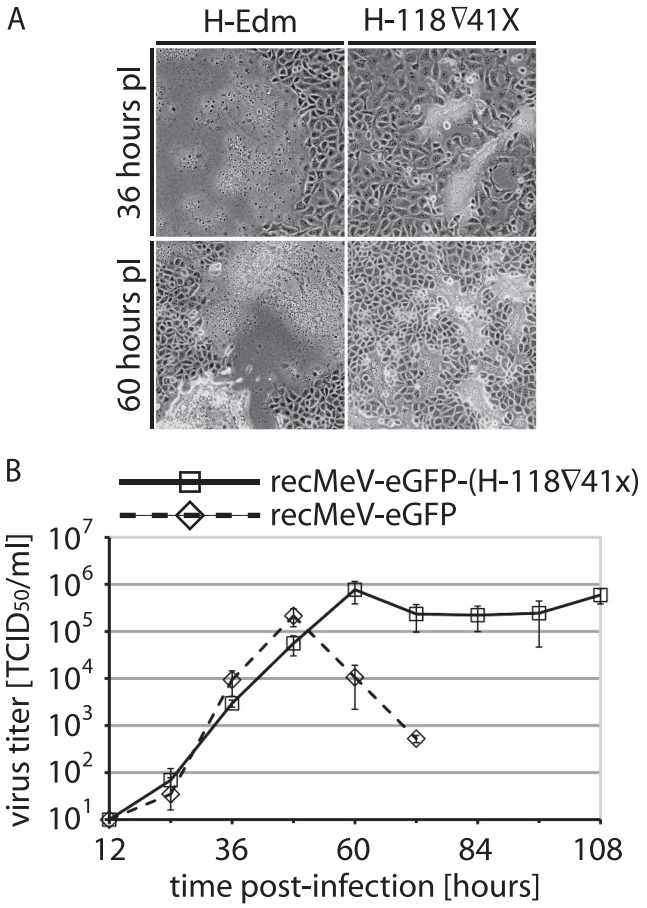

FIG. 7. The H-84∇41x variant harboring the 41-residue membrane-distal stalk insertion supports virus infection and growth. (A) Microphotographs (overlays of phase contrast and fluorescence) of Vero-SLAM cells infected with recombinant recMeV-eGFP-(H-118∇41x) that contains the H-118∇41x variant instead of normal H or unmodified recMeV-eGFP for comparison. Cells were infected at an MOI of 0.01 and photographed 36 and 60 h postinfection (pI) at a magnification of ×200. Representative fields of view are shown. (B) recMeV-eGFP-(H-118∇41x) growth curves show an extended plateau phase of peak titers of progeny virus. Vero-SLAM cells were infected with recMeV-eGFP-(H-118∇41x) or recMeV-eGFP at an MOI of 0.001, and titers of cell-associated viral particles were determined at the indicated time points through $TCID_{50}$ titration. Average values from three independent experiments are shown, and error bars represent SDs.

and growth in comparison to standard recMeV-eGFP. Figure 7A shows that cell-to-cell fusion was also the predominant CPE associated with the recMeV-eGFP-(H-118∇41x) variant. However, final syncytial sizes were reduced, and the incubation time until syncytial disintegration was increased compared to that for the recMeV-eGFP variant. These observations were corroborated by multiple-step viral growth curves. The recMeV-eGFP-(H-118∇41x) variant grew efficiently to final titers equivalent to those reached by the recMeV-eGFP variant (Fig. 7B). However, presumably due to reduced lateral spread and, hence, less-rapid breakdown of syncytia in cell culture, recMeV-eGFP-(H-118∇41x) growth curves showed an extended plateau phase of high virus titers, as opposed to the sharp drop from the peak titer observed for the recMeV-eGFP variant (Fig. 7B).

These data confirm that our observations based on transient expression of H-118∇41x and F are fully transferable to the context of virus infection. Thus, they underscore that an H stalk elongation of approximately 50%, inserted membrane distal to residue 118, is compatible with productive interaction of H with the prefusion F trimer and the efficient formation of infectious particles.

DISCUSSION

With an increasing number of high-resolution X-ray structures of envelope glycoproteins of paramyxovirinae at hand, elucidating the spatial organization of functional fusion complexes in situ has emerged as a major task in better understanding the molecular mechanism of infection by paramyxovirinae. In this study, we subjected key predictions derived from hypothetical glycoprotein interaction models that were generated on the basis of crystallographic and biochemical data (14, 16, 28, 36, 43, 77) to experimental evaluation. In aggregate, our results suggest a spatial ectodomain organization in which the prefusion F head domain contacts a membrane-distal section of the H stalk. This requires positioning of the H head domain above prefusion F in a staggered-head alignment. Several lines of evidence support these conclusions.

First, N-glycan shielding at H stalk position 111 blocks both functional and physical glycoprotein interactions, suggesting close proximity of F to this section of the H stalk. While these results could alternatively derive from a long-range, indirect effect of the added glycans, efficient H-111-Nglyc surface expression, unchanged receptor binding capacity, and a rigid α-helical configuration of the stalk supported by secondary structure predictions (36, 43) and circular dichroism analysis of the related HPIV5 HN stalk (78) render this unlikely. Nearly unperturbed physical interaction and F triggering capacity of H-72-Nglyc underscore this conclusion. It is noteworthy in this context that additional N-glycosylation sites are efficiently recognized at three consecutive positions starting with residue 110 but only at position 72 of the more-membrane-proximal 70-to-72 triplet. This suggests that rotational flexibility within the postulated α-helical coiled coils is limited in proximity to the transmembrane domains but increases toward membrane-distal positions. Bulky N-glycans at any of the three membrane-distal positions and/or glycan-induced slight rotation of the stalk helix in the *z* axis may interrupt precise protein-protein contacts at the H and F interface.

Second, mutagenesis of individual residues around the previously identified H stalk section from positions 110 to 114 (36) has highlighted three residues (111, 114, and 118), predicted to be located on consecutive turns of the MeV H stalk α-helix as determinants of both effective F triggering and, in particular, in the case of residues 111 and 118, glycoprotein interaction. Previously, Corey and Iorio demonstrated that mutation of MeV H stalk residue I84, L92, I98, or I99 likewise affects F triggering (16). Based on very efficient coprecipitation of these mutants with F, they concluded that these residues likely contribute to F triggering through indirect effects or form one of several interaction domains. Since it is likely a requirement that the F trimer separates at some stage in fusion from the

attachment protein for F refolding to proceed (73, 74), increased strength of hetero-oligomer interaction might be sufficient to reduce or block fusion. While indirect effects could likewise result when an alanine point mutation is inserted at position 111, 114, or 118, the block of F triggering by these H variants combined with a strong reduction of glycoprotein interactions in situ makes it alternatively conceivable that these residues engage in short-range functional contacts required for the initiation of F refolding.

Lastly, shortening the MeV H stalk by either membrane-proximal or membrane-distal residues 84 to 117 blocks both hetero-oligomerization and triggering. This is compatible with both the parallel (required protein-protein contacts are disrupted)- and staggered (steric constraints between F head and a lowered H head)-alignment hypotheses of glycoprotein head domains. Importantly, though, increasing the length of the H stalk membrane proximal to residue 84 by only ~11 Å disrupts hetero-oligomerization and F triggering, while an insertion of the same length membrane distal to residue 118 still allows the formation of functional fusion complexes. This demonstrates that the position of the section from positions 84 to 118 relative to the donor membrane, and thus relative to the F trimer, is critical for productive hetero-oligomerization. Tolerance to stalk elongation at position 118 renders specific protein-protein contacts between the H head and F unlikely, in particular, since structurally rigid insertions with a predicted pitch of approximately 75 Å in an α-helical configuration are compatible with the formation of functional fusion complexes in the context of both transient glycoprotein expression and recombinant virus particles. This finding furthermore supports the idea that H and F oligomers separate after successful initiation of F rearrangements, given that in the case of continued hetero-oligomer interaction, the 75-Å H extension would likely keep the target membrane outside the range of the F fusion peptide.

The fact that large stalk insertions with very strong α-helical propensity are tolerated membrane distal to residue 118 furthermore lends support to secondary structure predictions (36) extending a rigid, helical configuration found for the PIV5 HN stalk (78) to MeV H. Insertions equivalent to 1.9 (7 residues), 3.9 (14 residues), or 11.4 (41 residues) helix turns are compatible with the formation of functional fusion complexes. This again suggests some rotational flexibility within the H stalk as considered above on the basis of successful insertion of N-glycans at positions 110, 111, and 112. A drop in F triggering and surface expression as a consequence of a 55-residue insertion supports, however, the idea that stalk insertions of progressive length eventually have a destabilizing effect on H.

If H stalks enjoy some rotational flexibility and residues in stalk section 84 to 118 (presumably residues 111, 114, and 118) engage in short-range contacts for F triggering, how is receptor binding by the H head domain (48, 71) signaled to the contact zone despite the presence of a long (41-residue) stalk insertion? Interestingly, no major conformational changes between crystal structures of PIV5 HN, HPIV3 HN, and henipavirus G, solved alone or in complex with their receptors, were observed (8, 9, 74). Although receptor binding was originally proposed to initiate major changes in the NDV HN protein (17, 61, 62), subsequent work has demonstrated that major HN rearrangements are unlikely to be required for NDV F triggering (39). Since the dimer-of-dimer interface of PIV5 HN is substantially smaller than that within the dimer interaction, it has been hypothesized as a possible mechanism for F triggering that receptor binding may result in partial disassembly of the tetrameric head of the HN attachment protein, in turn changing the interaction with F and inducing triggering (78). Some conformational changes upon receptor binding have also been implicated for Nipah virus and Hendra virus G (1, 4). For the latter, it was proposed that these changes may affect the dimer-of-dimer interface (6).

By analogy, partial or complete disintegration of hypothetical MeV H homotetramers upon receptor binding would not require complex signaling through the stalk domain and, thus, be reconcilable with the partially maintained functionality of the H-118▽41x variant. However, isolated MeV H head domain fragments have crystallized as monomers (14) and homodimers (28). In this context, it should be noted that similarly soluble head domains of henipavirus G attachment proteins are also monomeric in solution and crystals (8, 74). Nevertheless, native G is predicted to exist in a tetrameric dimer-of-dimers configuration (7). Elucidating the order of physiological, membrane-embedded MeV H oligomers before and after receptor binding therefore emerges as a central task in understanding the mechanism of MeV F triggering. While we represent H structures as homodimers in this study for simplicity and in light of the available X-ray data, we remain open to the hypothesis that the tetramer constitutes the physiological oligomer of MeV H. Certainly, reorganization of a hypothetical dimer-of-dimer oligomer rather than an intricate signaling mechanism could provide a straightforward explanation as to how engagement of distinct binding sites in the H-Edm head domain by CD46 or SLAM (48, 71), and even of single-chain antibody moieties carboxy-terminally attached to MeV H through flexible linkers (27), results in effective F triggering.

ACKNOWLEDGMENTS

We thank J. J. Yoon and A. Shapiro for help with support experiments of the study and A. L. Hammond for critical reading of the manuscript.

M.A.B. was funded by the Molecular Mechanisms of Microbial Pathogenesis training grant T32 AI007470 from the NIH. This work was supported by U.S. Public Health Service grant AI071002 (to R.K.P.) from the NIH/NIAID.

REFERENCES

1. **Aguilar, H. C., Z. A. Ataman, V. Aspericueta, A. Q. Fang, M. Stroud, O. A. Negrete, R. A. Kammerer, and B. Lee.** 2009. A novel receptor-induced activation site in the Nipah virus attachment glycoprotein (G) involved in triggering the fusion glycoprotein (F). J. Biol. Chem. **284:**1628–1635.
2. **Aguilar, H. C., K. A. Matreyek, C. M. Filone, S. T. Hashimi, E. L. Levroney, O. A. Negrete, A. Bertolotti-Ciarlet, D. Y. Choi, I. McHardy, J. A. Fulcher, S. V. Su, M. C. Wolf, L. Kohatsu, L. G. Baum, and B. Lee.** 2006. N-glycans on Nipah virus fusion protein protect against neutralization but reduce membrane fusion and viral entry. J. Virol. **80:**4878–4889.
3. **Ben-Efraim, I., Y. Kliger, C. Hermesh, and Y. Shai.** 1999. Membrane-induced step in the activation of Sendai virus fusion protein. J. Mol. Biol. **285:**609–625.
4. **Bishop, K. A., A. C. Hickey, D. Khetawat, J. R. Patch, K. N. Bossart, Z. Zhu, L. F. Wang, D. S. Dimitrov, and C. C. Broder.** 2008. Residues in the stalk domain of the Hendra virus G glycoprotein modulate conformational changes associated with receptor binding. J. Virol. **82:**11398–11409.
5. **Bishop, K. A., T. S. Stantchev, A. C. Hickey, D. Khetawat, K. N. Bossart, V. Krasnoperov, P. Gill, Y. R. Feng, L. Wang, B. T. Eaton, L. F. Wang, and C. C. Broder.** 2007. Identification of Hendra virus G glycoprotein residues that are critical for receptor binding. J. Virol. **81:**5893–5901.
6. **Bossart, K. N., and C. C. Broder.** 2008. Paramyxovirus entry. *In* S. Pohlmann and G. Simmons (ed.), Viral entry into host cells. Landes Bioscience, Austin, TX.

7. **Bossart, K. N., G. Crameri, A. S. Dimitrov, B. A. Mungall, Y. R. Feng, J. R. Patch, A. Choudhary, L. F. Wang, B. T. Eaton, and C. C. Broder.** 2005. Receptor binding, fusion inhibition, and induction of cross-reactive neutralizing antibodies by a soluble G glycoprotein of Hendra virus. J. Virol. **79:**6690–6702.
8. **Bowden, T. A., A. R. Aricescu, R. J. Gilbert, J. M. Grimes, E. Y. Jones, and D. I. Stuart.** 2008. Structural basis of Nipah and Hendra virus attachment to their cell-surface receptor ephrin-B2. Nat. Struct. Mol. Biol. **15:**567–572.
9. **Bowden, T. A., M. Crispin, D. J. Harvey, A. R. Aricescu, J. M. Grimes, E. Y. Jones, and D. I. Stuart.** 2008. Crystal structure and carbohydrate analysis of Nipah virus attachment glycoprotein: a template for antiviral and vaccine design. J. Virol. **82:**11628–11636.
10. **Buchholz, U. J., S. Finke, and K. K. Conzelmann.** 1999. Generation of bovine respiratory syncytial virus (BRSV) from cDNA: BRSV NS2 is not essential for virus replication in tissue culture, and the human RSV leader region acts as a functional BRSV genome promoter. J. Virol. **73:**251–259.
11. **Burkhard, P., R. A. Kammerer, M. O. Steinmetz, G. P. Bourenkov, and U. Aebi.** 2000. The coiled-coil trigger site of the rod domain of cortexillin I unveils a distinct network of interhelical and intrahelical salt bridges. Structure **8:**223–230.
12. **Cathomen, T., H. Y. Naim, and R. Cattaneo.** 1998. Measles viruses with altered envelope protein cytoplasmic tails gain cell fusion competence. J. Virol. **72:**1224–1234.
13. **Chen, L., J. J. Gorman, J. McKimm-Breschkin, L. J. Lawrence, P. A. Tulloch, B. J. Smith, P. M. Colman, and M. C. Lawrence.** 2001. The structure of the fusion glycoprotein of Newcastle disease virus suggests a novel paradigm for the molecular mechanism of membrane fusion. Structure (Cambridge) **9:**255–266.
14. **Colf, L. A., Z. S. Juo, and K. C. Garcia.** 2007. Structure of the measles virus hemagglutinin. Nat. Struct. Mol. Biol. **14:**1227–1228.
15. **Colman, P. M., and M. C. Lawrence.** 2003. The structural biology of type I viral membrane fusion. Nat. Rev. Mol. Cell Biol. **4:**309–319.
16. **Corey, E. A., and R. M. Iorio.** 2007. Mutations in the stalk of the measles virus hemagglutinin protein decrease fusion but do not interfere with virus-specific interaction with the homologous fusion protein. J. Virol. **81:**9900–9910.
17. **Crennell, S., T. Takimoto, A. Portner, and G. Taylor.** 2000. Crystal structure of the multifunctional paramyxovirus hemagglutinin-neuraminidase. Nat. Struct. Biol. **7:**1068–1074.
18. **Deng, R., A. M. Mirza, P. J. Mahon, and R. M. Iorio.** 1997. Functional chimeric HN glycoproteins derived from Newcastle disease virus and human parainfluenza virus-3. Arch. Virol. Suppl. **13:**115–130.
19. **Deng, R., Z. Wang, P. J. Mahon, M. Marinello, A. Mirza, and R. M. Iorio.** 1999. Mutations in the Newcastle disease virus hemagglutinin-neuraminidase protein that interfere with its ability to interact with the homologous F protein in the promotion of fusion. Virology **253:**43–54.
20. **Deng, R., Z. Wang, A. M. Mirza, and R. M. Iorio.** 1995. Localization of a domain on the paramyxovirus attachment protein required for the promotion of cellular fusion by its homologous fusion protein spike. Virology **209:**457–469.
21. **Dörig, R. E., A. Marcil, A. Chopra, and C. D. Richardson.** 1993. The human CD46 molecule is a receptor for measles virus (Edmonston strain). Cell **75:**295–305.
22. **Duprex, W. P., S. McQuaid, L. Hangartner, M. A. Billeter, and B. K. Rima.** 1999. Observation of measles virus cell-to-cell spread in astrocytoma cells by using a green fluorescent protein-expressing recombinant virus. J. Virol. **73:**9568–9575.
23. **Federspiel, M. J., and S. H. Hughes.** 1998. Retroviral gene delivery, p. 179–214. *In* C. P. Emerson and H. L. Sweeney (ed.), Methods in cell biology, vol. 52. Academic Press, San Diego, CA.
24. **Gallagher, P., J. Henneberry, I. Wilson, J. Sambrook, and M. J. Gething.** 1988. Addition of carbohydrate side chains at novel sites on influenza virus hemagglutinin can modulate the folding, transport, and activity of the molecule. J. Cell Biol. **107:**2059–2073.
25. **Gravel, K. A., and T. G. Morrison.** 2003. Interacting domains of the HN and F proteins of Newcastle disease virus. J. Virol. **77:**11040–11049.
26. **Griffin, D. E.** 2007. Measles virus, p. 1551–1585. *In* D. M. Knipe and P. M. Howley (ed.), Fields virology, 5th ed., vol. 1. Lippincott Williams & Wilkins, Philadelphia, PA.
27. **Hammond, A. L., R. K. Plemper, J. Zhang, U. Schneider, S. J. Russell, and R. Cattaneo.** 2001. Single-chain antibody displayed on a recombinant measles virus confers entry through the tumor-associated carcinoembryonic antigen. J. Virol. **75:**2087–2096.
28. **Hashiguchi, T., M. Kajikawa, N. Maita, M. Takeda, K. Kuroki, K. Sasaki, D. Kohda, Y. Yanagi, and K. Maenaka.** 2007. Crystal structure of measles virus hemagglutinin provides insight into effective vaccines. Proc. Natl. Acad. Sci. USA **104:**19535–19540.
29. **Hu, X. L., R. Ray, and R. W. Compans.** 1992. Functional interactions between the fusion protein and hemagglutinin-neuraminidase of human parainfluenza viruses. J. Virol. **66:**1528–1534.
30. **Iorio, R. M., and P. J. Mahon.** 2008. Paramyxoviruses: different receptors—different mechanisms of fusion. Trends Microbiol. **16:**135–137.
31. **Jain, S., L. W. McGinnes, and T. G. Morrison.** 2008. Overexpression of thiol/disulfide isomerases enhances membrane fusion directed by the Newcastle disease virus fusion protein. J. Virol. **82:**12039–12048.
32. **Lamb, R. A., and T. S. Jardetzky.** 2007. Structural basis of viral invasion: lessons from paramyxovirus F. Curr. Opin. Struct. Biol. **17:**427–436.
33. **Lamb, R. A., and G. D. Parks.** 2007. Paramyxoviridae: the viruses and their replication, p. 1449–1496. *In* D. M. Knipe and P. M. Howley (ed.), Fields virology, 5th ed., vol. 1. Lippincott Williams & Wilkins, Philadelphia, PA.
34. **Lamb, R. A., R. G. Paterson, and T. S. Jardetzky.** 2006. Paramyxovirus membrane fusion: lessons from the F and HN atomic structures. Virology **344:**30–37.
35. **Lawrence, M. C., N. A. Borg, V. A. Streltsov, P. A. Pilling, V. C. Epa, J. N. Varghese, J. L. McKimm-Breschkin, and P. M. Colman.** 2004. Structure of the haemagglutinin-neuraminidase from human parainfluenza virus type III. J. Mol. Biol. **335:**1343–1357.
36. **Lee, J. K., A. Prussia, T. Paal, L. K. White, J. P. Snyder, and R. K. Plemper.** 2008. Functional interaction between paramyxovirus fusion and attachment proteins. J. Biol. Chem. **283:**16561–16572.
37. **Lee, J. K., A. Prussia, J. P. Snyder, and R. K. Plemper.** 2007. Reversible inhibition of the fusion activity of measles virus F protein by an engineered intersubunit disulfide bridge. J. Virol. **81:**8821–8826.
38. **Ludwig, K., B. Schade, C. Bottcher, T. Korte, N. Ohlwein, B. Baljinnyam, M. Veit, and A. Herrmann.** 2008. Electron cryomicroscopy reveals different F1+F2 protein states in intact parainfluenza virions. J. Virol. **82:**3775–3781.
39. **Mahon, P. J., A. M. Mirza, T. A. Musich, and R. M. Iorio.** 2008. Engineered intermonomeric disulfide bonds in the globular domain of the Newcastle disease virus hemagglutinin-neuraminidase protein: implications for the mechanism of fusion promotion. J. Virol. **82:**10386–10396.
40. **Manchester, M., D. S. Eto, A. Valsamakis, P. B. Liton, R. Fernandez-Munoz, P. A. Rota, W. J. Bellini, D. N. Forthal, and M. B. Oldstone.** 2000. Clinical isolates of measles virus use CD46 as a cellular receptor. J. Virol. **74:**3967–3974.
41. **McGinnes, L., T. Sergel, and T. Morrison.** 1993. Mutations in the transmembrane domain of the HN protein of Newcastle disease virus affect the structure and activity of the protein. Virology **196:**101–110.
42. **McGinnes, L. W., and T. G. Morrison.** 2006. Inhibition of receptor binding stabilizes Newcastle disease virus HN and F protein-containing complexes. J. Virol. **80:**2894–2903.
43. **Melanson, V. R., and R. M. Iorio.** 2006. Addition of N-glycans in the stalk of the Newcastle disease virus HN protein blocks its interaction with the F protein and prevents fusion. J. Virol. **80:**623–633.
44. **Melanson, V. R., and R. M. Iorio.** 2004. Amino acid substitutions in the F-specific domain in the stalk of the Newcastle disease virus HN protein modulate fusion and interfere with its interaction with the F protein. J. Virol. **78:**13053–13061.
45. **Melikyan, G. B., R. M. Markosyan, H. Hemmati, M. K. Delmedico, D. M. Lambert, and F. S. Cohen.** 2000. Evidence that the transition of HIV-1 gp41 into a six-helix bundle, not the bundle configuration, induces membrane fusion. J. Cell Biol. **151:**413–423.
46. **Naniche, D., G. Varior-Krishnan, F. Cervoni, T. F. Wild, B. Rossi, C. Rabourdin-Combe, and D. Gerlier.** 1993. Human membrane cofactor protein (CD46) acts as a cellular receptor for measles virus. J. Virol. **67:**6025–6032.
47. **Navaratnarajah, C. K., V. H. Leonard, and R. Cattaneo.** 2009. Measles virus glycoprotein complex assembly, receptor attachment, and cell entry. Curr. Top. Microbiol. Immunol. **329:**59–76.
48. **Navaratnarajah, C. K., S. Vongpunsawad, N. Oezguen, T. Stehle, W. Braun, T. Hashiguchi, K. Maenaka, Y. Yanagi, and R. Cattaneo.** 2008. Dynamic interaction of the measles virus hemagglutinin with its receptor signaling lymphocytic activation molecule (SLAM, CD150). J. Biol. Chem. **283:**11763–11771.
49. **Ng, D. T., S. W. Hiebert, and R. A. Lamb.** 1990. Different roles of individual N-linked oligosaccharide chains in folding, assembly, and transport of the simian virus 5 hemagglutinin-neuraminidase. Mol. Cell. Biol. **10:**1989–2001.
50. **Ng, D. T., R. E. Randall, and R. A. Lamb.** 1989. Intracellular maturation and transport of the SV5 type II glycoprotein hemagglutinin-neuraminidase: specific and transient association with GRP78-BiP in the endoplasmic reticulum and extensive internalization from the cell surface. J. Cell Biol. **109:**3273–3289.
51. **Oldstone, M. B., D. Homann, H. Lewicki, and D. Stevenson.** 2002. One, two, or three step: measles virus receptor dance. Virology **299:**162–163.
52. **Ono, N., H. Tatsuo, Y. Hidaka, T. Aoki, H. Minagawa, and Y. Yanagi.** 2001. Measles viruses on throat swabs from measles patients use signaling lymphocytic activation molecule (CDw150) but not CD46 as a cellular receptor. J. Virol. **75:**4399–4401.
53. **Peisajovich, S. G., O. Samuel, and Y. Shai.** 2000. Paramyxovirus F1 protein has two fusion peptides: implications for the mechanism of membrane fusion. J. Mol. Biol. **296:**1353–1365.
54. **Plemper, R. K., A. L. Hammond, and R. Cattaneo.** 2000. Characterization of a region of the measles virus hemagglutinin sufficient for its dimerization. J. Virol. **74:**6485–6493.
55. **Plemper, R. K., A. L. Hammond, and R. Cattaneo.** 2001. Measles virus

envelope glycoproteins hetero-oligomerize in the endoplasmic reticulum. J. Biol. Chem. **276:**44239–44246.
56. **Plemper, R. K., A. L. Hammond, D. Gerlier, A. K. Fielding, and R. Cattaneo.** 2002. Strength of envelope protein interaction modulates cytopathicity of measles virus. J. Virol. **76:**5051–5061.
57. **Prussia, A. J., R. K. Plemper, and J. P. Snyder.** 2008. Measles virus entry inhibitors: a structural proposal for mechanism of action and the development of resistance. Biochemistry **47:**13573–13583.
58. **Radecke, F., P. Spielhofer, H. Schneider, K. Kaelin, M. Huber, C. Dotsch, G. Christiansen, and M. A. Billeter.** 1995. Rescue of measles viruses from cloned DNA. EMBO J. **14:**5773–5784.
59. **Spearman, C.** 1908. The method of right and wrong cases (constant stimuli) without Gauss's formula. Br. J. Psychol. **2:**227–242.
60. **Sutter, G., M. Ohlmann, and V. Erfle.** 1995. Non-replicating vaccinia vector efficiently expresses bacteriophage T7 RNA polymerase. FEBS Lett. **371:**9–12.
61. **Takimoto, T., G. L. Taylor, H. C. Connaris, S. J. Crennell, and A. Portner.** 2002. Role of the hemagglutinin-neuraminidase protein in the mechanism of paramyxovirus-cell membrane fusion. J. Virol. **76:**13028–13033.
62. **Takimoto, T., G. L. Taylor, S. J. Crennell, R. A. Scroggs, and A. Portner.** 2000. Crystallization of Newcastle disease virus hemagglutinin-neuraminidase glycoprotein. Virology **270:**208–214.
63. **Tanabayashi, K., and R. W. Compans.** 1996. Functional interaction of paramyxovirus glycoproteins: identification of a domain in Sendai virus HN which promotes cell fusion. J. Virol. **70:**6112–6118.
64. **Tatsuo, H., N. Ono, K. Tanaka, and Y. Yanagi.** 2000. SLAM (CDw150) is a cellular receptor for measles virus. Nature **406:**893–897.
65. **Tatsuo, H., N. Ono, and Y. Yanagi.** 2001. Morbilliviruses use signaling lymphocyte activation molecules (CD150) as cellular receptors. J. Virol. **75:**5842–5850.
66. **Thompson, S. D., W. G. Laver, K. G. Murti, and A. Portner.** 1988. Isolation of a biologically active soluble form of the hemagglutinin-neuraminidase protein of Sendai virus. J. Virol. **62:**4653–4660.
67. **Tomasi, M., C. Pasti, C. Manfrinato, F. Dallocchio, and T. Bellini.** 2003. Peptides derived from the heptad repeat region near the C-terminal of Sendai virus F protein bind the hemagglutinin-neuraminidase ectodomain. FEBS Lett. **536:**56–60.
68. **Tsuchiya, E., K. Sugawara, S. Hongo, Y. Matsuzaki, Y. Muraki, Z. N. Li, and K. Nakamura.** 2002. Effect of addition of new oligosaccharide chains to the globular head of influenza A/H2N2 virus haemagglutinin on the intracellular transport and biological activities of the molecule. J. Gen. Virol. **83:**1137–1146.
69. **Tsurudome, M., M. Ito, M. Nishio, M. Kawano, K. Okamoto, S. Kusagawa, H. Komada, and Y. Ito.** 1998. Identification of regions on the fusion protein of human parainfluenza virus type 2 which are required for haemagglutinin-neuraminidase proteins to promote cell fusion. J. Gen. Virol. **79:**279–289.
70. **Tsurudome, M., M. Kawano, T. Yuasa, N. Tabata, M. Nishio, H. Komada, and Y. Ito.** 1995. Identification of regions on the hemagglutinin-neuraminidase protein of human parainfluenza virus type 2 important for promoting cell fusion. Virology **213:**190–203.
71. **Vongpunsawad, S., N. Oezgun, W. Braun, and R. Cattaneo.** 2004. Selectively receptor-blind measles viruses: identification of residues necessary for SLAM- or CD46-induced fusion and their localization on a new hemagglutinin structural model. J. Virol. **78:**302–313.
72. **Wang, Z., A. M. Mirza, J. Li, P. J. Mahon, and R. M. Iorio.** 2004. An oligosaccharide at the C-terminus of the F-specific domain in the stalk of the human parainfluenza virus 3 hemagglutinin-neuraminidase modulates fusion. Virus Res. **99:**177–185.
73. **White, J. M., S. E. Delos, M. Brecher, and K. Schornberg.** 2008. Structures and mechanisms of viral membrane fusion proteins: multiple variations on a common theme. Crit. Rev. Biochem. Mol. Biol. **43:**189–219.
74. **Xu, K., K. R. Rajashankar, Y. P. Chan, J. P. Himanen, C. C. Broder, and D. B. Nikolov.** 2008. Host cell recognition by the henipaviruses: crystal structures of the Nipah G attachment glycoprotein and its complex with ephrin-B3. Proc. Natl. Acad. Sci. USA **105:**9953–9958.
75. **Yao, Q., X. Hu, and R. W. Compans.** 1997. Association of the parainfluenza virus fusion and hemagglutinin-neuraminidase glycoproteins on cell surfaces. J. Virol. **71:**650–656.
76. **Yin, H. S., R. G. Paterson, X. Wen, R. A. Lamb, and T. S. Jardetzky.** 2005. Structure of the uncleaved ectodomain of the paramyxovirus (hPIV3) fusion protein. Proc. Natl. Acad. Sci. USA **102:**9288–9293.
77. **Yin, H. S., X. Wen, R. G. Paterson, R. A. Lamb, and T. S. Jardetzky.** 2006. Structure of the parainfluenza virus 5 F protein in its metastable, prefusion conformation. Nature **439:**38–44.
78. **Yuan, P., G. P. Leser, B. Demeler, R. A. Lamb, and T. S. Jardetzky.** 2008. Domain architecture and oligomerization properties of the paramyxovirus PIV 5 hemagglutinin-neuraminidase (HN) protein. Virology **378:**282–291.
79. **Yuan, P., T. B. Thompson, B. A. Wurzburg, R. G. Paterson, R. A. Lamb, and T. S. Jardetzky.** 2005. Structural studies of the parainfluenza virus 5 hemagglutinin-neuraminidase tetramer in complex with its receptor, sialyllactose. Structure **13:**803–815.
80. **Zhao, X., M. Singh, V. N. Malashkevich, and P. S. Kim.** 2000. Structural characterization of the human respiratory syncytial virus fusion protein core. Proc. Natl. Acad. Sci. USA **97:**14172–14177.